

Chapter 2

Interleaver

2.1 Introduction

An interleaver is a periodic optical filter that can combine or separate a comb of dense wavelength-division multiplexed (DWDM) signals. The original design separates (or combines) even channels from odd channels across a DWDM comb. The filter function of an interleaver and its period are separable. Interleavers have been demonstrated that resolve a comb of DWDM frequencies on 100 GHz, 50 GHz, 25 GHz, and 12.5 GHz centers. The period is governed by the free-spectral range of the core elements, where narrower channel spacing is achieved by a longer optical path. The design goals for the passband are a wide, flat (or nearly) top with minimum insertion loss (IL) and rapid roll off on the band edges. The chromatic dispersion across the passband is to be minimized. On a wideband level there are a work to alignment between the comb of DWDM frequencies (nominally allocated on the ITU grid (Table. 3.2)) and filter function of the interleaver [2.1]. Generally, the free-spectral range (FSR) of the interleaving filter is not accurately matched to the ITU grid and the center frequencies of the channels still may be offset error.

There are three broad classes of interleaver filter technologies: lattice filter (LF), Gires-Tournois (GT) [2.2] based Michelson interferometer, and arrayed-waveguide touter (AWG). This chapter will introduce the theory and design process of the GT and the LF interleavers. Design tolerance was also estimated by Monte-Carlo simulation.

In the chapter-three, the all interleaver models used by simulation system don't consider the sellmeier equation of the birefringent crystal. Because that we don't want to care about many variables in our simulation system to confirm the model

accuracy.

2.2 Digital Concepts for Optical Filters

Digital filter, or discrete time filter [2.3], has been widely used in digital electronic circuit. The desired filter is generally implemented with digital computation and used to filter a signal that is derived from a continuous-time signal by means of periodic sampling followed by analog-to-digital conversion. Borrowed from the electronic world, optical engineer follows the same concept and uses optical delay line to create the desired filter function. Before describing the design process of the interleaver filter, the basic knowledge about the representations of digital signals, the Z-transform, the zeros, and the poles were needed to be introduced in followed sub-sections.

2.2.1 Discrete Signals and Z-transform [2.4]

A discrete signal can be obtained by sampling a continuous time signal $x(t)$ at $t = nT$ where the sampling interval is, T and n is the sample number. For a digital filter, T is the unit delay associated with the discrete impulse response. The impulse response of an optical filter, where each stage has a delay that is an integer multiple of the unit delay, is described by a discrete sequence. The Fourier transform of a sequence has a sum instead of an integral as follows:

$$X(f) = \sum_{n=-\infty}^{\infty} x(nT)e^{-j2\pi fnT} \quad (1)$$

where f denote the absolute frequency. A normalized frequency is defined as $\nu \equiv fT = f / FSR$, where the free spectral range (FSR) is the period of the absolute frequency response. The normalized angular frequency is given by $\omega = 2\pi\nu$. A discrete signal is often represented by $x(n)$, leaving T implied. The discrete-time Fourier transform (DTFT) is defined as

$$X(\nu) = \sum_{n=-\infty}^{\infty} x(n)e^{-j2\pi\nu n} \quad (2)$$

The Z-transform is an analytic extension of the DTFT for discrete signals, similar to the relationship between the Laplace transform and the Fourier transform for continuous signals [2.4]. The Z-transform is defined for a discrete signal by substituting z for $e^{j\omega}$ in Eq. (2) as follows:

$$H(z) = \sum_{n=-\infty}^{\infty} h(n)z^{-n} \quad (3)$$

where $h(n)$ is the impulse response of a filter or the values of a discrete signal, and z is a complex number that may have any magnitude. For the power series to be meaningful, a region of convergence must be specified, for example $r_{\min} \leq |z| \leq r_{\max}$.

The particular interest is $|z|=1$, called the unit circle, because the filter's frequency response is found by evaluating $H(z)$ along $z = e^{j\omega}$. The inverse Z-transform is found by applying the Cauchy integral theorem to Eq. (3) to obtain:

$$h(n) = \frac{1}{2\pi j} \oint H(z)z^{n-1} dz \quad (4)$$

The convolution resulting from filtering in the time domain

$$y(n) = x(n) * h(n) = \sum_{m=-\infty}^{\infty} x(m)h(n-m) \quad (5)$$

reduces to multiplication in the Z-domain.

$$Y(z) = H(z)X(z) \quad (6)$$

Equation (6) shows that a filter's transfer function, $H(z)$, can be obtain by dividing the output by the input in the Z-domain.

$$H(z) = \frac{Y(z)}{X(z)} \quad (7)$$

A fundamental property of the Z-transform relates $h(n-1)$ to $H(z)$ as shown in Eq. (8)

$$\sum_{n=-\infty}^{\infty} h(n-1)z^{-n} = z^{-1} \sum_{n=-\infty}^{\infty} h(n)z^{-n} = z^{-1}H(z) \quad (8)$$

The impulse response is assumed to be causal [2.3] so that $h(n) = 0$ for $n < 0$.

One delay results in multiplication by z^{-1} in the Z-domain, and N delays results in multiplication by z^{-N} .

The Z-transforms are introduced for two example here. First, let the output of a filter be the sum of the last $N + 1$ inputs: $y(n) = x(n) + x(n-1) + \dots + x(n-N)$. Such a filter contains N delays, which are feed-forward paths. The impulse response is $h(n) = \delta(n) + \delta(n-1) + \dots + \delta(n-N)$.

The transfer function is $H(z) = 1 + z^{-1} + \dots + z^{-N} = (1 - z^{-(N+1)}) / (1 - z^{-1})$.

There are N roots of $H(z)$ which all occur on the unit circle. For second example, let the output of a filter be given as $y(n) = ay(n-1) + x(n)$, where a is a real number satisfying $0 \leq |a| < 1$ and $n \geq 0$. This filter contains one delay, which is a feedback path. Its Z-transform is $Y(z) = az^{-1}Y(z) + X(z)$, which gives the transfer function $H(z) = Y(z) / X(z) = 1 / (1 - az^{-1})$. The transfer function is equivalent to the infinite sum

$$H(z) = \sum_{n=-\infty}^{\infty} a^n z^{-n} = \frac{1}{1 - az^{-1}} \quad (9)$$

The region of convergence is $|z| > a$.

2.2.2 Poles and Zeros

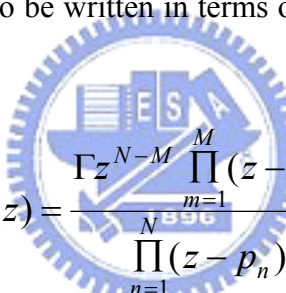
A discrete linear system with a discrete input signal in Eq. (10) as follows:

$$y(n) = b_0x(n) + b_1x(n-1) + \dots + b_Mx(n-M) - a_1y(n-1) - \dots - a_Ny(n-N) \quad (10)$$

The weights are given by the a and b coefficients. The Z-transform results in a transfer function that is a ratio of polynomials.

$$H(z) = \frac{\sum_{m=0}^M b_m z^{-m}}{1 + \sum_{n=1}^N a_n z^{-n}} = \frac{B(z)}{A(z)} \quad (11)$$

$A(z)$ and $B(z)$ are M th and N th-order polynomials, respectively. The expression for $H(z)$ can also be written in terms of the roots of the polynomials as follows [2.5]:



$$H(z) = \frac{\Gamma z^{N-M} \prod_{m=1}^M (z - z_m)}{\prod_{n=1}^N (z - p_n)} \quad (12)$$

The zeros of the numerator are represented by z_m . A zero that occurs on the unit circle, $|z_m| = 1$, results in zero transmission at that frequency. The roots of the denominator polynomial are designed by p_n . The Γ has a maximum value determined by $\max\{|H(z)|_{z=e^{j\omega}}\} = 1$.

Digital filters are classified by the polynomials defined in Eq. (11). A moving average (MA) filter has only zeros and also belongs to a finite impulse response. It consists only of feed-forward paths. A single stage MA digital filter is shown in Figure 2.1(a). An autoregressive (AR) filter has only poles and contains one or more feedback paths as shown in Fig. 2.1(b). A pole produces an impulse response with

an infinite number of terms in contrast to the finite number of terms for MA filters.

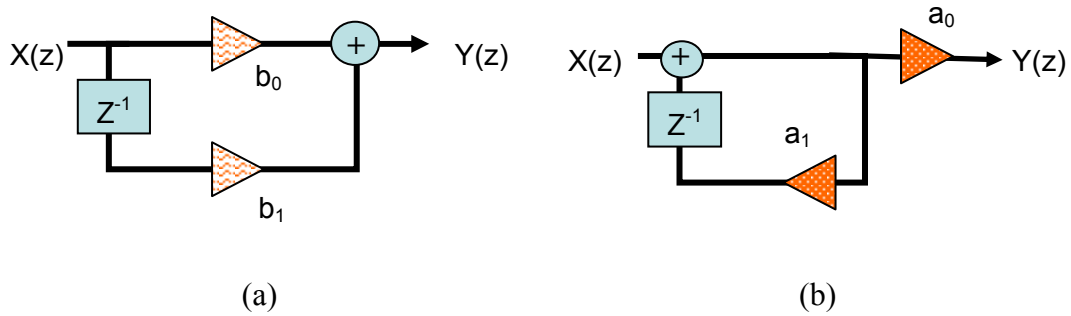


Fig. 2.1 Illustrations of single-stage (a) MA digital filter and (b) AR digital filter.

2.2.3 Magnitude Response and Group Delay

A filter's magnitude response is equal to $|H(z)|$ evaluated at $z = e^{j\omega}$. Based on Eq. (11), the distance of each pole and zero from the unit circle affects the magnitude response, i.e. $|e^{j\omega} - z_m|$ or $|e^{j\omega} - p_n|$. A convenient graphical method for estimating a filter's magnitude response is the pole-zero diagram as shown in Fig. 2.2. Zeros are designated by o 's and poles by x 's. One trip around the unit circle is equal to one FSR. Zeros with a magnitude >1 are called maximum-phase, and those with magnitudes <1 are called minimum-phase. A pole-zero diagram with a pair of zeros that are located reciprocally about the unit circle is shown in Fig. 2.3.

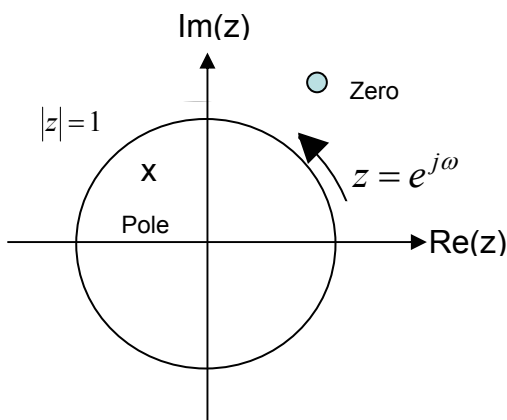


Fig. 2.2 Pole-zero diagram showing the unit circle, one pole, and one zero.

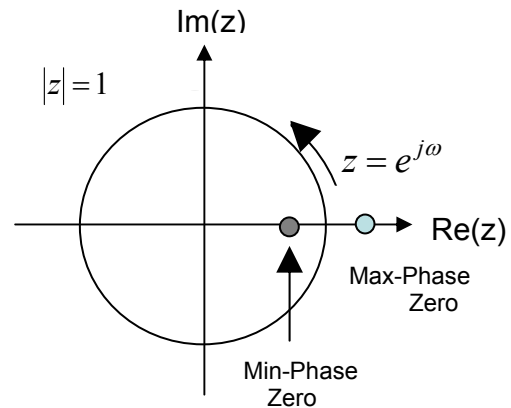


Fig. 2.3 Pole-zero diagram showing a maximum- and a minimum-phase zero.

The filter's group delay is defined as the negative derivative of the phase of the transfer function with respect to the angular frequency as follows [2.5]:

$$\tau_g = T \times \tau_n = T \times \left[-\frac{d}{d\omega} \tan^{-1} \left(\frac{\text{Im}\{H(z)\}}{\text{Re}\{H(z)\}} \right) \right]_{z=e^{j\omega}} \quad (13)$$

where τ_n is normalized to the unit delay, T. To obtain the group delay for a single zero, consider the transfer function $H_{1-zero}(z) = 1 - re^{j\phi}z^{-1}$ where r and ϕ are the magnitude and phase of the zero. By substituting $z = e^{j\omega}$ in $H_{1-zero}(z)$, the phase is derived in terms of r , ϕ , and ω as follows:

$$\Phi_{1-zero} = \tan^{-1} \left[\frac{r \sin(\omega - \phi)}{1 - r \cos(\omega - \phi)} \right] \quad (14)$$

$$\frac{d \tan^{-1}[g(x)]}{dx} = \frac{g'(x)}{1 + g^2(x)} \quad (15)$$

where Φ_{1-zero} is the phase of $H_{1-zero}(z)$. Borrowed from Eq. (15), the group delay simplifies to

$$\tau_{1-zero}(r, \phi) = \frac{r[r - \cos(\omega - \phi)]}{1 - 2r \cos(\omega - \phi) + r^2} \quad (16)$$

Then, consider the transfer function, $H_{1-zero}(z) = re^{-j\phi} - z^{-1}$, with the reversed path, the group delay is

$$\tau_{1-zero}\left(\frac{1}{r}, \phi\right) = \frac{[1 - r \cos(\omega - \phi)]}{1 - 2r \cos(\omega - \phi) + r^2} = 1 - \tau_{1-zero}(r, \phi) \quad (17)$$

The sum of the group delays is a constant value indicating that the filter has linear phase with the same magnitude response as shown in Fig. 2.4.

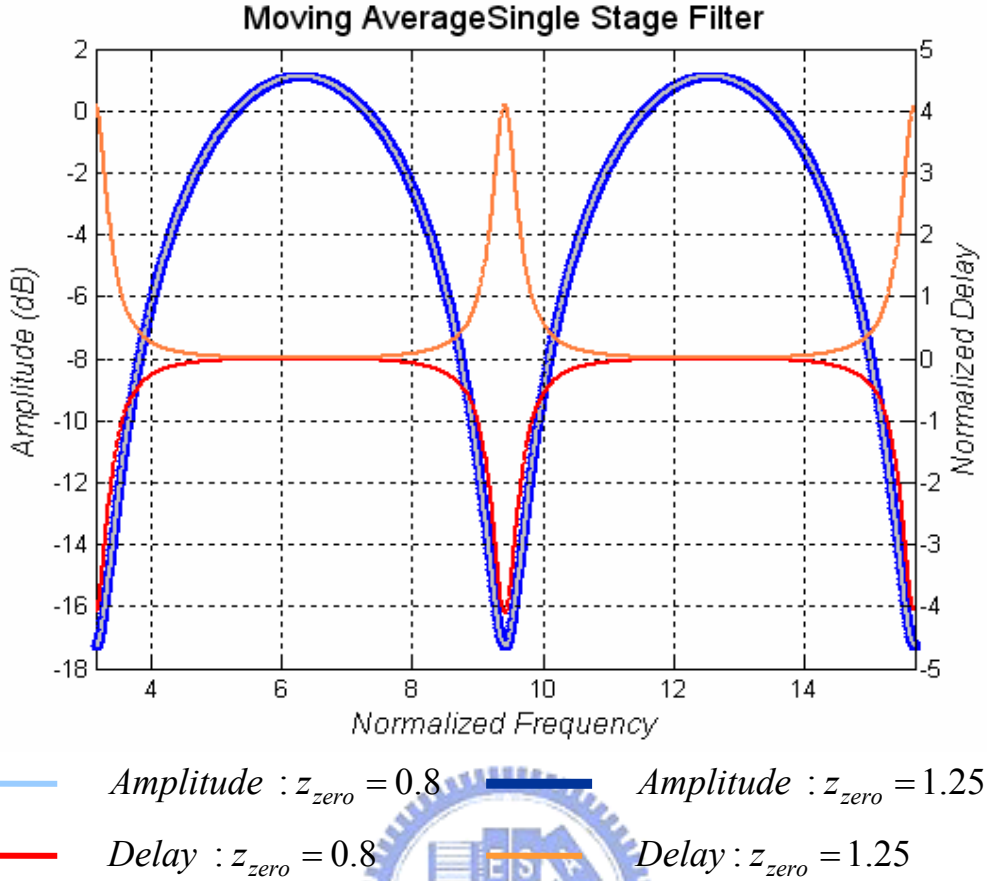


Fig. 2.4 Phase response of maximum and minimum phase MA filters.

2.3 Interleaver

2.3.1 Michelson Gires-Tournois (GT) Interleaver

As shown in Fig. 2.5, the popular optical bandpass filter is a modified Michelson interferometer in which one of its reflecting mirrors is replaced by GT-resonator (GTR) with a cavity spacing d . A light beam injected into this filter is split into two beams of equal intensity by the beamsplitter (BS: $r = 1/\sqrt{2}, t = 1/\sqrt{2}$) [2.6]. One beam shown horizontally in the figure, $j/\sqrt{2}a_1$, travels to the right mirror (mirror3) and is returned with the phase factor $-e^{-j2kL_2}$, where $k = \omega/c$. Another one beam, $1/\sqrt{2}a_1$, propagates vertically through arm L_1 and is reflected back by GT resonator. They are recombined at the “output” side of the mirror to

produce b_2 :

$$b_2 = \frac{j}{\sqrt{2}} \frac{1}{\sqrt{2}} e^{-j2kL_2} a_1 + \frac{j}{\sqrt{2}} e^{-jkL_1} S_{11}^{GTR} \frac{1}{\sqrt{2}} e^{-jkL_1} a_1 \quad (18)$$

where S_{11}^{GTR} is a element of the scattering matrix of the Fabry-Perot interferometer (GT- resonator here) as shown in Eq. (19).

$$S_{11}^{GTR} = \frac{-(r_1 - r_2 e^{-j\delta})}{(1 - r_1 r_2 e^{-j\delta}) \times (-t_1 t_2 e^{-j\delta/2})} \quad (19)$$

where t_1 and t_2 are the transmissivity of mirror 1 and mirror 2, respectively.

$$t = \sqrt{1 - r^2} \quad (20)$$

And the transmission beam travels from M_1 to M_2 , this path increase the phase shifted by $\omega nd / c \equiv \delta / 2$.

According the Eq. (18), this device have the potential dynamic characteristics, 1) tunable center-wavelength and 2) variable bandwidth. If the parameter d and $\Delta L (= L_1 - L_2)$ can be changed, then the center-wavelength of the bandpass function can be tuned continuously as shown in Fig. 2.5. The initial resonator spacing, d_0 , is set to $2000\lambda_0$ in order to give a channel spacing of 100GHz with 50GHz bandwidth where $\lambda_0 = 1.54 \mu m$. Note that compared with d_0 , the variation of d , Δd , is very smaller. The second dynamic feature is its variable bandwidth as shown in Fig. 2.6. This can be achieved if the variation of d is not constraint by the condition ($d_0 \gg \Delta d$).

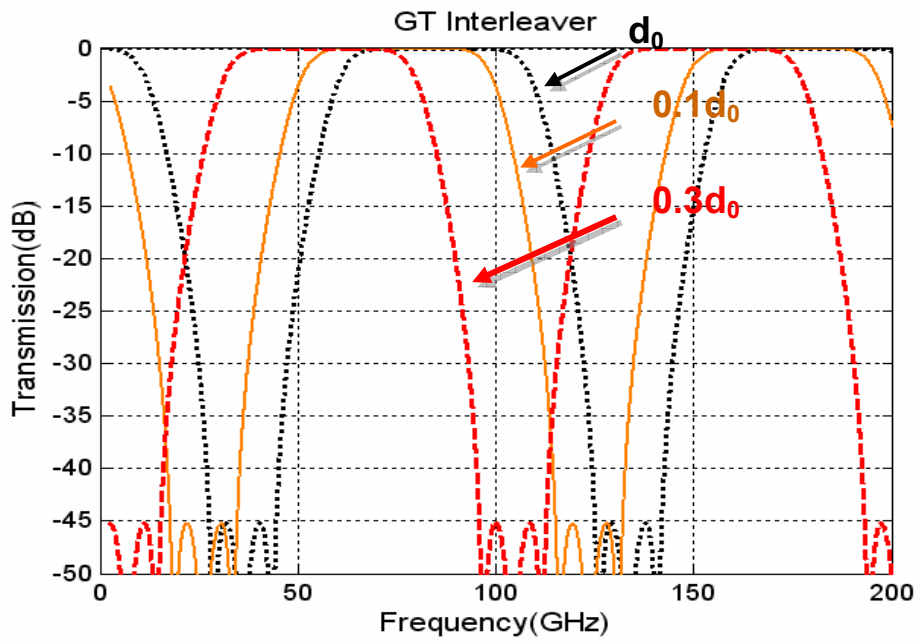


Fig. 2.5 The transmitted intensity showing the tunable characteristic of center-wavelength.

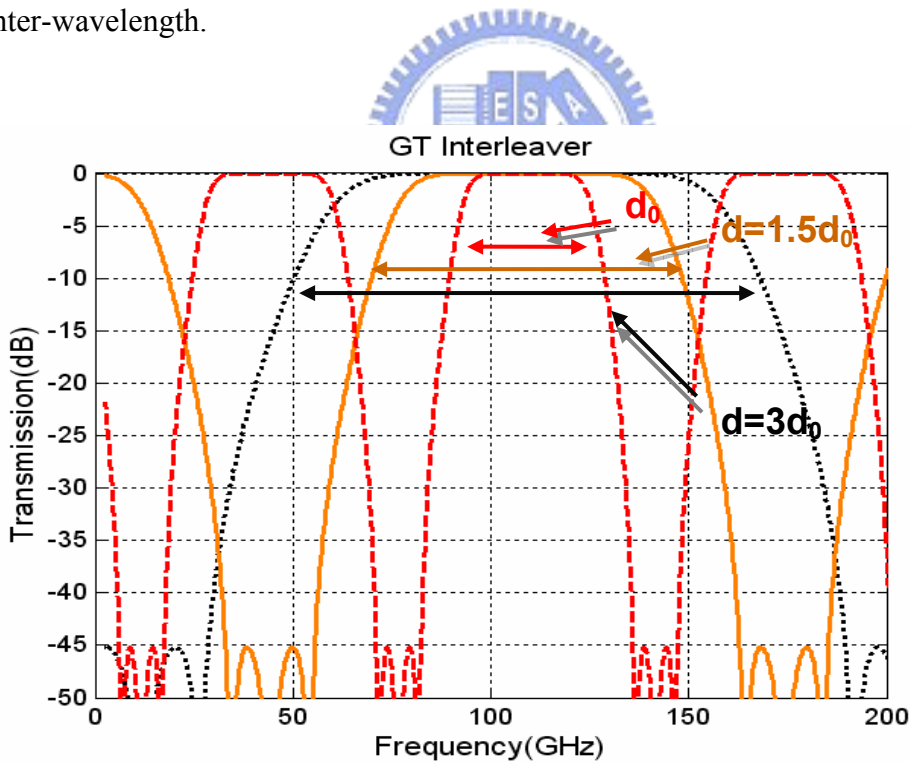


Fig. 2.6 The transmitted intensity showing the variable bandwidth capacity.

The phase response of this type filter comes from a combination of a linear term

$k(L_1 + L_2)$ and a nonlinear term due to GTR response as shown in Fig. 2.7. Note that the GTR filter has a pole and contains one feedback path as demonstrated by the single-stage digital filter is shown in Fig. 2.1(b) before. Since the pole magnitude must always be less than one for stability, poles contribute positive group delay [2.4]. Therefore, it is very difficult to find any filter with negative group delay to perfectly compensate the GTR with positive group delay and it is also a biggest defect in DWDM optical systems with the dispersion effect.

2.3.2 Lattice Interleaver

Figure 2.7 shows the configuration of the interleaver consisted of the birefringent crystals. Its basic theory is to generate the interference between polarized light, which depends on phase retardation between the components of light polarized parallel to the slow and the fast axes of the crystal. Therefore, the birefringent crystal is used as an optical delay line, and a half-wave plate is used to rotation the polarization in order to assign the components of two axes.

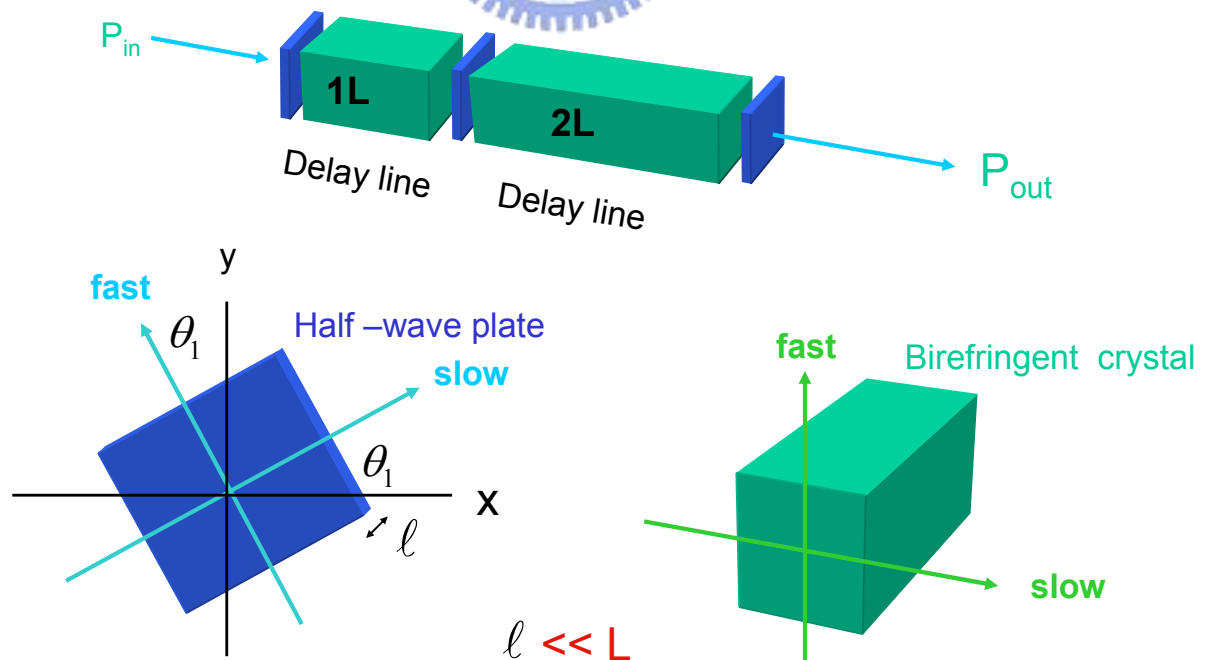
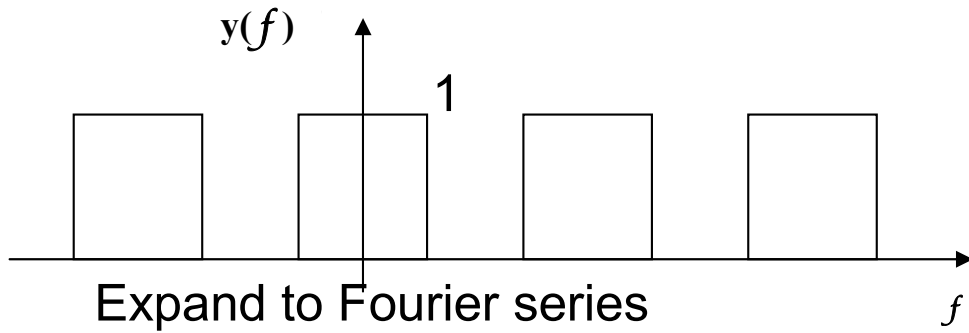
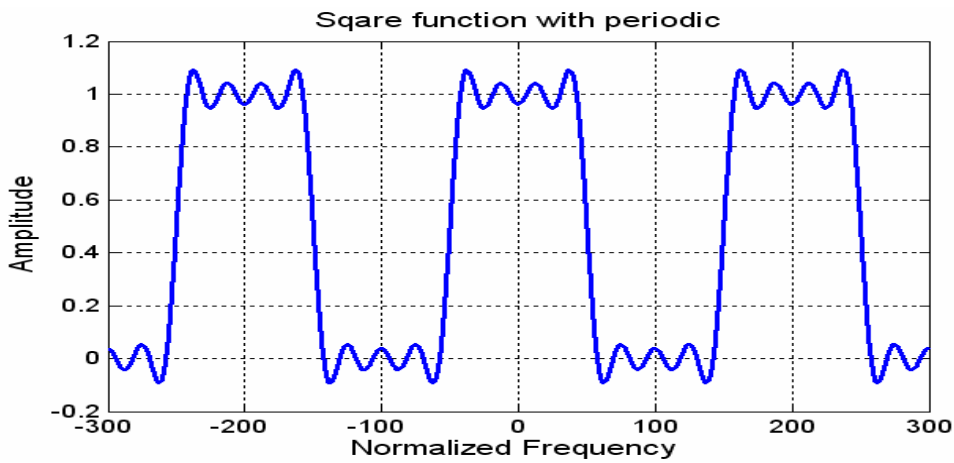


Fig. 2.7 Brief configuration of an L-2L interleaver

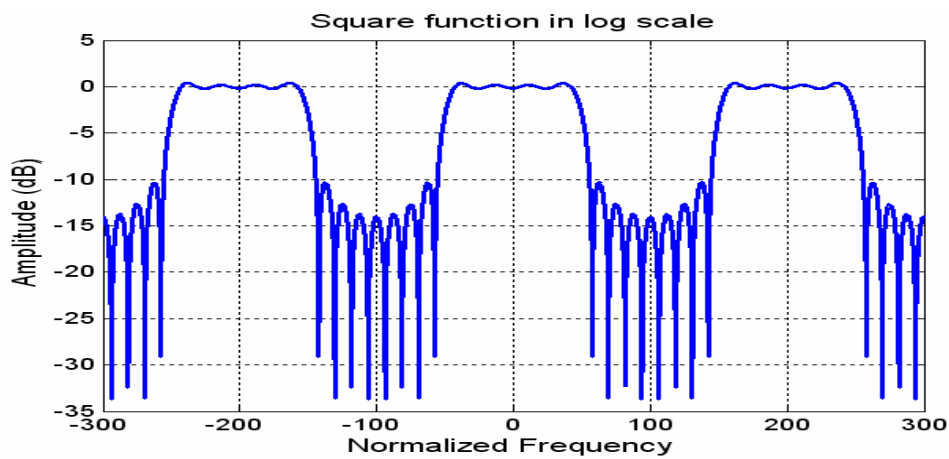
Actually, the goal of design is to generate a periodic rectangular function as shown in Fig. 2.8(a).



(a)



(b)



(c)

Fig. 2.8 The Fourier series function with periodic.

The function could be defined to

$$y(f) = \begin{cases} 0 & , -100 < f < -50 \\ 1 & , -50 < f < 50 \\ 0 & , -50 < f < 100 \end{cases} \quad , \quad y(f) = y(f + 200) \quad (21)$$

Expand it to a Fourier series, there is no even function term in it. The constant a_0 and a_n is retained.

$$a_0 = \frac{1}{200} \int_{-50}^{50} 1 \cdot df = \frac{1}{2} \quad (22)$$

$$a_n = \frac{1}{100} \int_{-50}^{50} 1 \cdot \cos(n2\pi f) \cdot df = \frac{2}{n\pi} \sin\left(\frac{n\pi}{2}\right) \quad , \quad n = 1, 2, 3 \dots$$

Then the final rectangular function will be written to the Eq. (23) and be plotted to the Fig. 2.8(b)-(c) with $n = 1, 3, 5, 7$.

$$y(f) = \frac{1}{2} + a_1 \cdot \cos(2\pi f) - a_3 \cdot \cos(3 \times 2\pi f) + \dots \quad (23)$$

Here we know that the square-wave amplitude function has only odd Fourier frequency components with appropriate Fourier coefficients.

According to the Jones matrix theory [2.7], a half-wave plate has a phase retardation of $\Gamma = \pi$, and the thickness of $\ell = \lambda / 2(n_e - n_o)$. The Jones matrix for the half-wave plate is obtained by using Eq. 24.

$$W_{hp} = \begin{bmatrix} 0 & -i \\ -i & 0 \end{bmatrix} \quad (24)$$

We can write the Jones matrix for the delay line as

$$W_{delay-line} = \begin{bmatrix} e^{-i\frac{\omega}{2}dnL} & 0 \\ 0 & e^{i\frac{\omega}{2}dnL} \end{bmatrix} \quad (25)$$

where L is the length of the delay-line crystal and dn is the difference between the n_e and n_o (the group indices of the ordinary and extraordinary axes). By

combining all Jones matrices of the birefringent crystals, we can write the transmission as

$$E_{out} = W_{hp}(22.5^\circ) * W_{2L}(\omega) * W_{hp}(\theta_2) * W_L(\omega/2) * W_{hp}(\theta_1) * E_{in} \quad (26)$$

where W_{2L} and W_L are the Jones matrices of the two crystals as shown in Fig. 2.9.

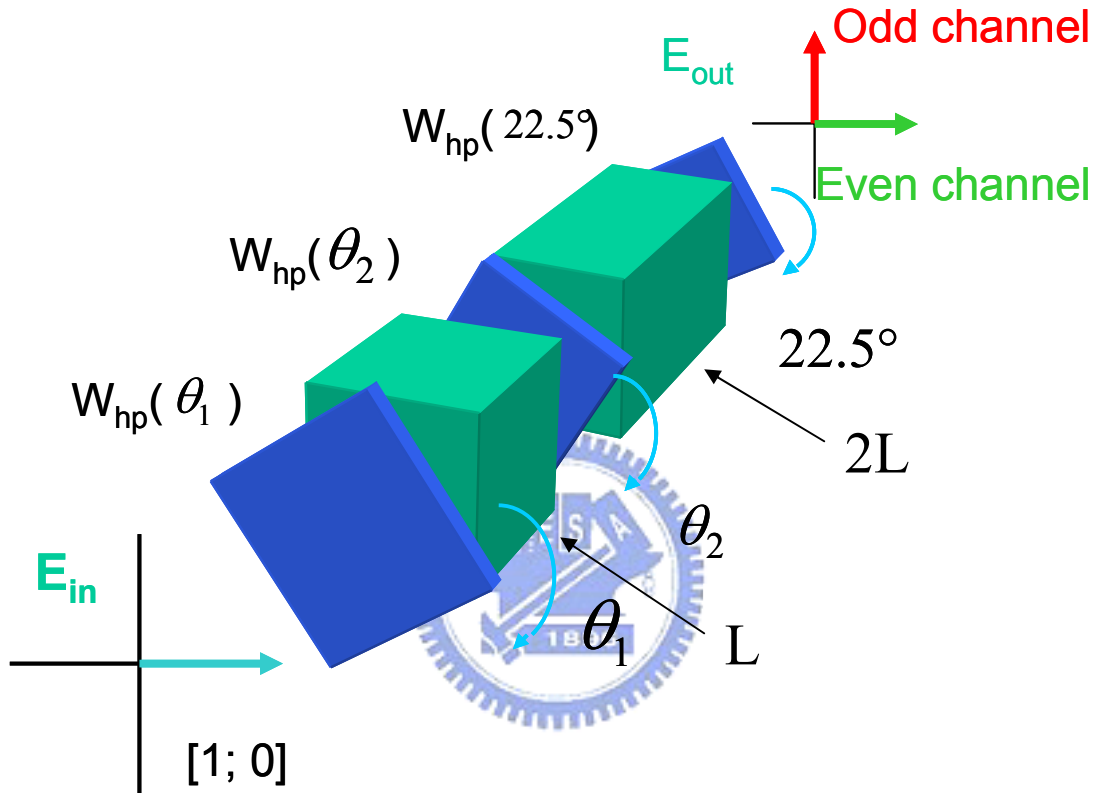


Fig. 2.9 To create the odd channels and even channels by rotating the half-wave plates.

In Fig. 2.9, the Jones matrix for the incident beam can be written as $[1;0]$. According to adjust appropriately the angles of the half-wave plates, we can get the odd channels and even channels lying the vertical and horizontal axes, respectively, at the output port. But the problem is how to get the angles to fit the Fourier coefficients in Eq. (22)? The answer is that we can use the optimization tools in Matlab programs. The goal is minimizing the error function by sweeping the half-wave plate angles as

$$\begin{aligned}
error &= \max |y(w) - x(w)| \\
error &= \int_{w_1}^{w_2} |y(w) - x(w)| dw \\
error &= \int_{w_1}^{w_2} |y(w) - x(w)|^2 dw \quad w_1 = w_c - \frac{FSR}{2}, w_2 = w_c + \frac{FSR}{2} \quad (27) \\
error &= \int_{w_1}^{w_2} \left| \log_{10}^{y(w)^2} - x(w) \right|^2 dw
\end{aligned}$$

where $x(w)$ is the target or ideal square periodic function and the $f(w)$ is real transmission function. The transmission function is periodic, so the errors are only summed over one FSR at the central frequency, w_c [2.8]. The first approximation criterion is based on the maximum error, which occurs at only one frequency for each $y(w)$. The last three approximation criteria include errors at all points of frequency in the interval; therefore, they include more error data than the first for each $y(w)$ considered. We choose the last approximation criterion because it is the energy in the error signal [2.9].

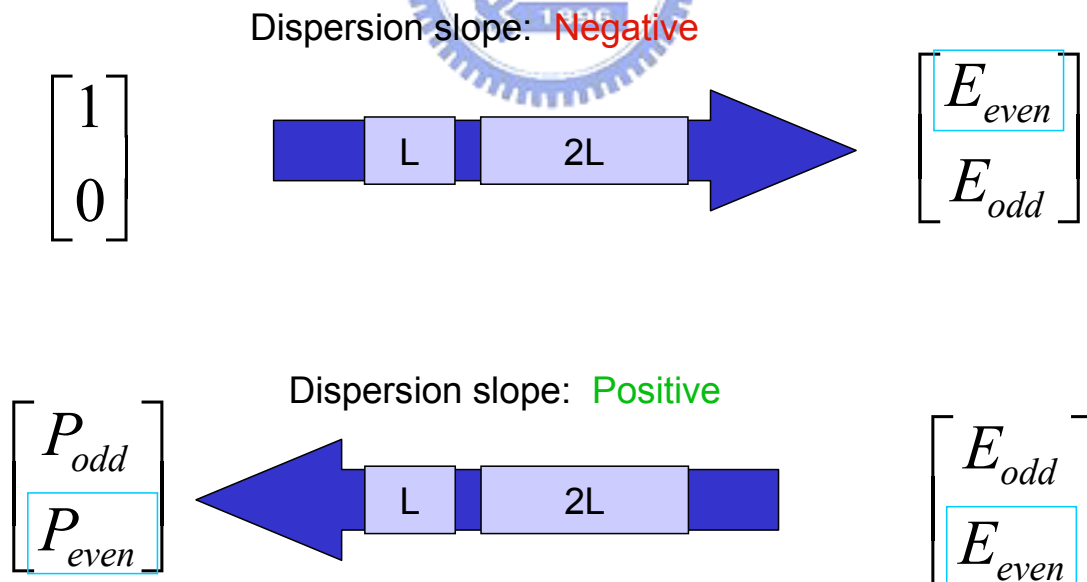


Fig. 2.10 Dispersion free path

Figure 2.10 shows the opposite slopes of the dispersion from the opposite paths.

The key point is to exchange the positions of E_{even} and E_{odd} , and get them into the

opposite direction.

2.3.3 Mathematical Derivation

Here we use the easiest case: one stage interleaver includes a delay line and two half-wave plates in which the second plate is determined to 22.5 degree. Assume

that there is a incident beam $V_x (= \begin{bmatrix} 1 \\ 0 \end{bmatrix})$ injected to the first half-wave plate, then the

Jones matrix M_1 at the output can be written as

$$\begin{aligned}
 M_1 &= \begin{bmatrix} \cos \theta_1 & -\sin \theta_1 \\ \sin \theta_1 & \cos \theta_1 \end{bmatrix} \cdot \begin{bmatrix} e^{-j\frac{\pi}{2}} & 0 \\ 0 & e^{j\frac{\pi}{2}} \end{bmatrix} \cdot \begin{bmatrix} \cos \theta_1 & -\sin \theta_1 \\ \sin \theta_1 & \cos \theta_1 \end{bmatrix} \cdot \begin{bmatrix} 1 \\ 0 \end{bmatrix} \\
 &= \begin{bmatrix} e^{-j\frac{\pi}{2}} \cos^2 \theta_1 + e^{j\frac{\pi}{2}} \sin^2 \theta_1 \\ e^{-j\frac{\pi}{2}} \cos \theta_1 \sin \theta_1 - e^{j\frac{\pi}{2}} \cos \theta_1 \sin \theta_1 \end{bmatrix} = j \cdot \begin{bmatrix} a_1(\theta_1) \\ a_2(\theta_2) \end{bmatrix} \quad (28) \\
 &\dots\dots(a_1 \text{ and } a_2 \text{ are real numbers})
 \end{aligned}$$

if the undetermined angle is set to be a variable θ_1 . Regard M_1 as the emerging beam and let it inject into the crystal of length L. The new Jones matrix M_2 is obtained by using Eq. (29).

$$M_2 = e^{-j\phi} \cdot \begin{bmatrix} e^{-j\frac{\pi f}{df_c}} & 0 \\ 0 & e^{j\frac{\pi f}{df_c}} \end{bmatrix} \cdot j \cdot \begin{bmatrix} a_1 \\ a_2 \end{bmatrix} = j \cdot \begin{bmatrix} a_1 e^{-j\frac{\pi f}{df_c}} \\ a_2 e^{j\frac{\pi f}{df_c}} \end{bmatrix} \quad (29)$$

In Eq. (29), df_c is the channel spacing and ϕ is equal to $dn\omega L / 2c$. The phase factor $e^{-j\phi}$ can be neglected if interference effects are not important, or not observable [2.7]. Then use M_2 to multiply the second half-wave plate

($W_{22.5^\circ} = j \begin{bmatrix} X & Y \\ Y & -X \end{bmatrix}$, X and Y are real numbers) with the angle of 22.5 degree

as shown in Eq. (30).

$$\begin{aligned}
M_3 &= W_{22.5^\circ} \cdot M_2 = j \begin{bmatrix} X & Y \\ Y & -X \end{bmatrix} \cdot j \begin{bmatrix} a_1 e^{-j\frac{\pi f}{df_c}} \\ a_2 e^{j\frac{\pi f}{df_c}} \end{bmatrix} \\
&= - \begin{bmatrix} a_1 X e^{-j\frac{\pi f}{df_c}} + a_2 Y e^{j\frac{\pi f}{df_c}} \\ a_1 X e^{-j\frac{\pi f}{df_c}} - a_2 Y e^{j\frac{\pi f}{df_c}} \end{bmatrix} = \begin{bmatrix} E_x \\ E_y \end{bmatrix}
\end{aligned} \tag{30}$$

In Eq. (30), we arbitrarily choose E_x or E_y and square it to obtain the Eq. (31).

$$\begin{aligned}
T &= E_x \cdot E_x^* = (a_1 X + a_2 Y)^2 \cos^2 \frac{\pi f}{df_c} + (a_1 X - a_2 Y)^2 \sin^2 \frac{\pi f}{df_c} \\
&= [a_1(\theta_1)X]^2 + \left\{ [a_2(\theta_2)Y]^2 + 2a_1(\theta_1)Xa_2(\theta_1)Y \right\} \cos \frac{2\pi f}{df_c}
\end{aligned} \tag{31}$$

Compare with Eq. (23), the first term needs to equal 1/2 and the coefficient of the second term needs to equal the Fourier coefficient by optimizing the angle of θ_1 .

By this way, we can easy to understand the theory of interleaver.

2.3.4 Interleaver Simulation Results

There are four kinds of interleaver filters consisted of L-2L, L-2L-2L, L-2L-4L, and L-2L-2L-2L delay lines in this section. The lengths of delay-line crystals in the program are determined using Eq. (32).

$$\begin{aligned}
f_c &= m \frac{c}{dnL} \Rightarrow L = \frac{f_c dn}{mc} \\
df_c &= \text{Channel spacing} = \text{FSR}
\end{aligned} \tag{32}$$

In Eq. (28), c is the speed of light; f_c is the central frequency in the range of operation frequencies; m is the order of the birefringent wave plate.

1. L-2L Interleaver

The found angles for two half-wave plates are 7.7356 and 29.5286 degrees.

Figure 2.11 shows the transmission responses of the even and odd channels; the isolation is about 30.5 dB.

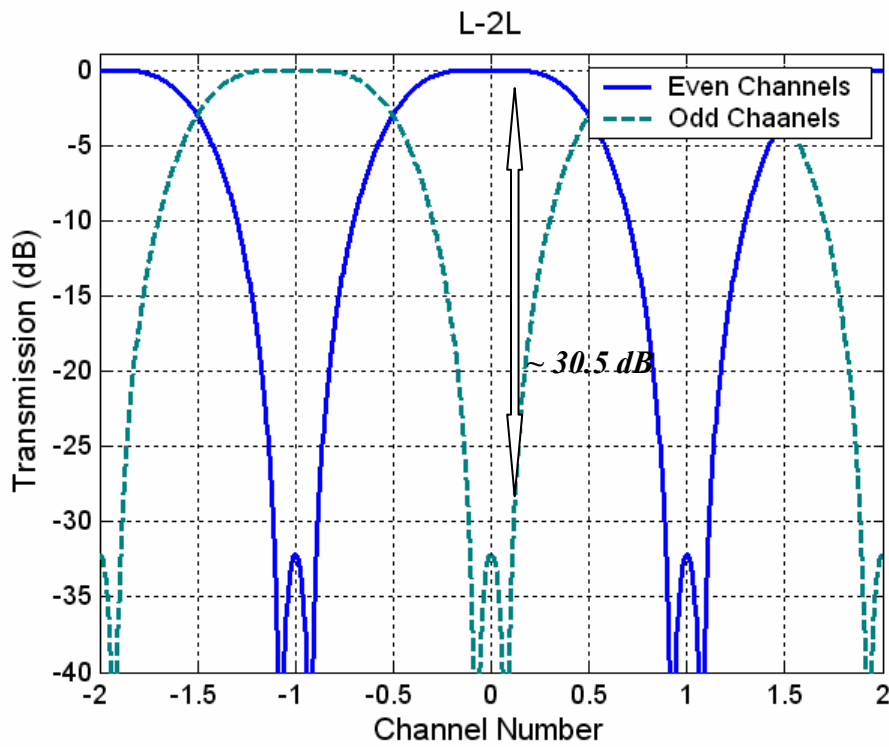


Fig. 2.11 Transmission responses of the even and odd channels.

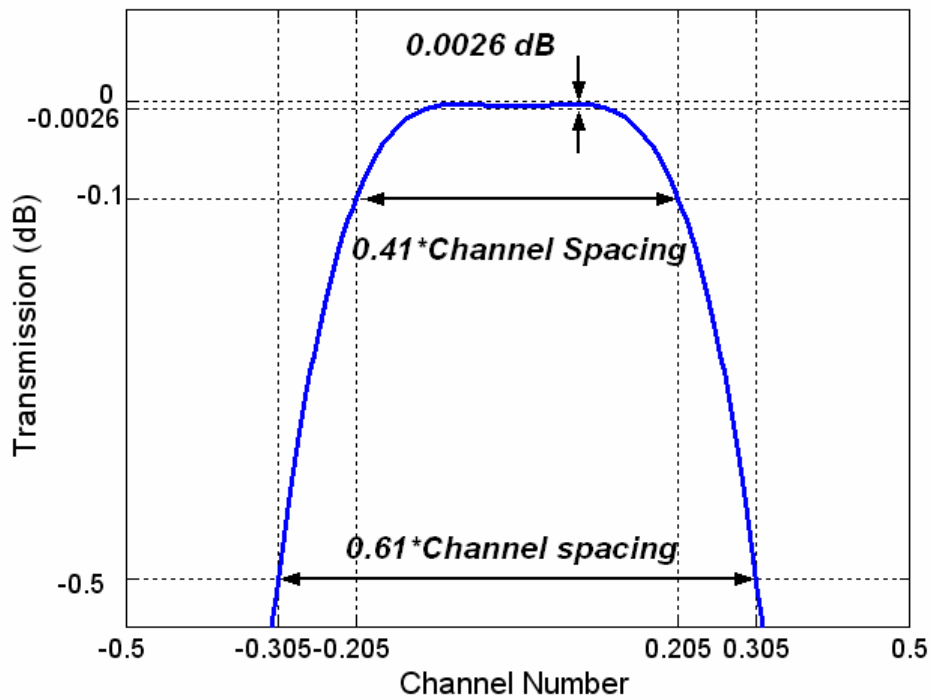


Fig. 2.12 The ripple calculation and the bandwidth estimations of -0.1dB and -0.5dB for L-2L interleaver.

The ripple is about 0.0026 dB; the bandwidths of -0.1dB and -0.5dB are $0.41 * df$ (channel spacing) and $0.61 * df$, respectively, as shown in Fig. 2.12.

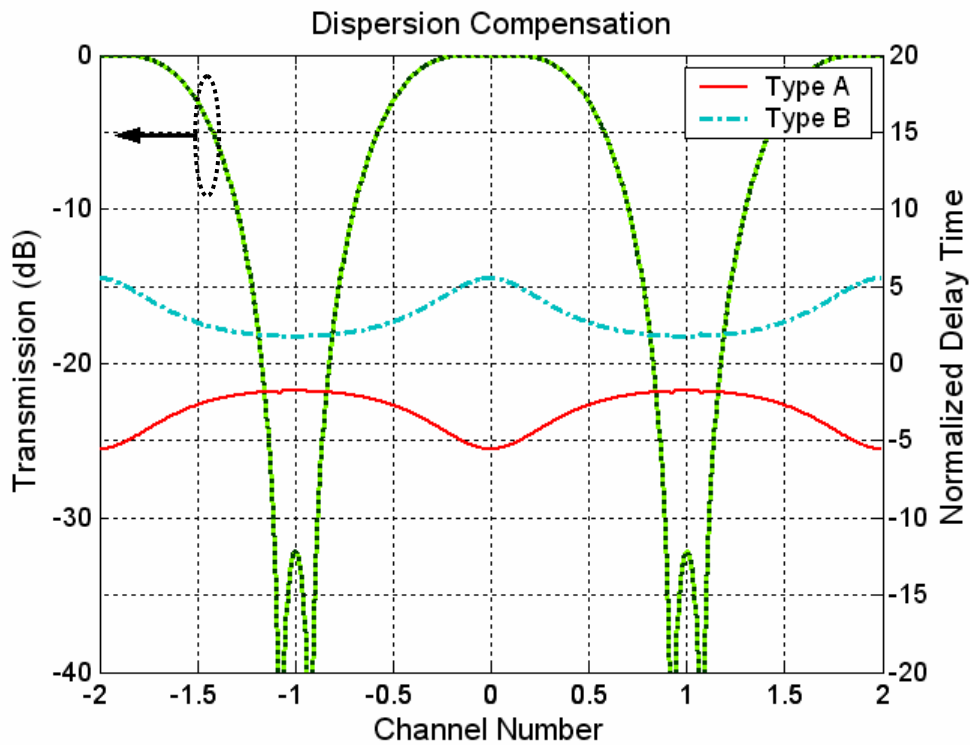


Fig. 2.13 Dispersion compensating interleavers for add/drop node

In Fig. 2.13, the path with the negative group delay is called type-A here, and another path with the positive group delay is called type-B. The type-A and type-B have the same transmission response.

2. *L-2L-2L Interleaver*

The found angles for three half-wave plates are 3.75, 13.75, and 31.7500 degrees. Figure 2.14 shows the transmission responses of the even and odd channels; the isolation is about 27 dB. The ripple is about 0.0049 dB; the bandwidths of -0.1dB and -0.5dB are $0.58 * df$ and $0.72 * df$, respectively, as shown in Fig. 2.15. In Fig. 2.16, the type-A and type-B have opposite group delays and company with the same transmission response.

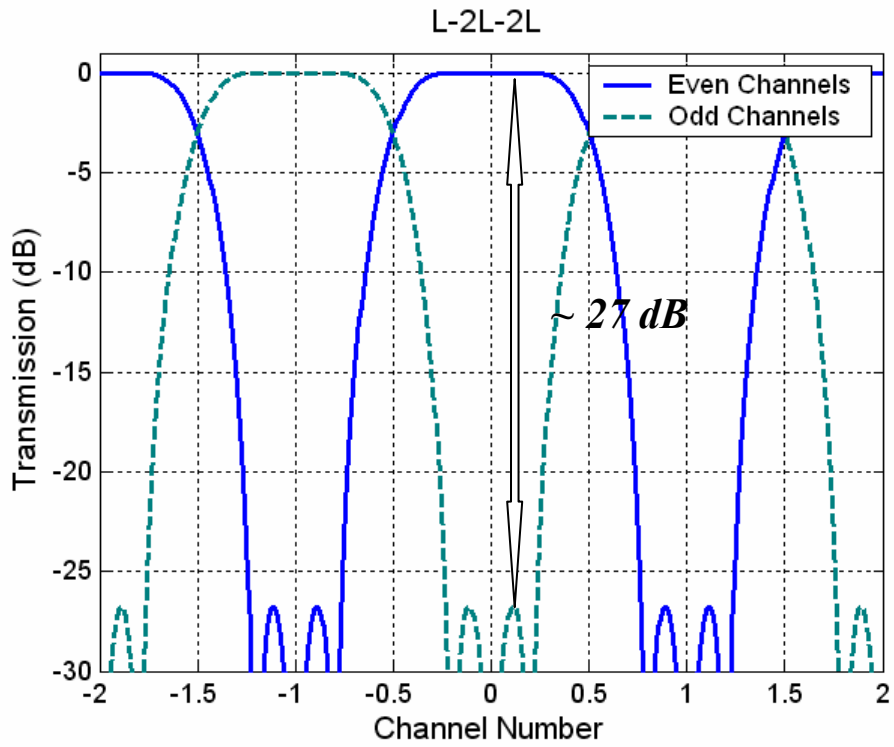


Fig. 2.14 Transmission responses of the even and odd channels

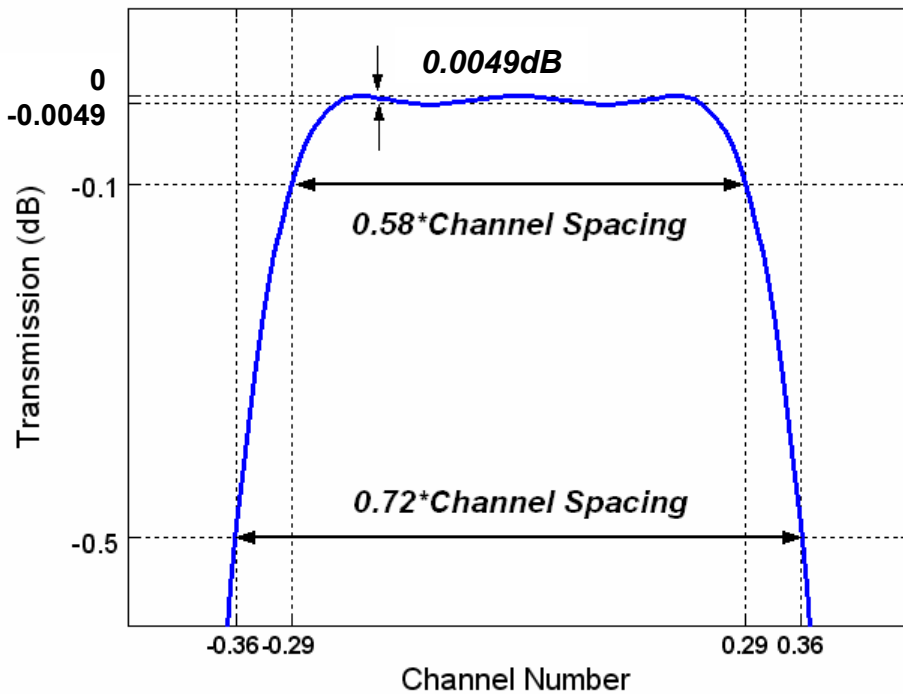


Fig. 2.15 The ripple calculation and the bandwidth estimations of -0.1dB and -0.5dB for L-2L-2L interleaver.

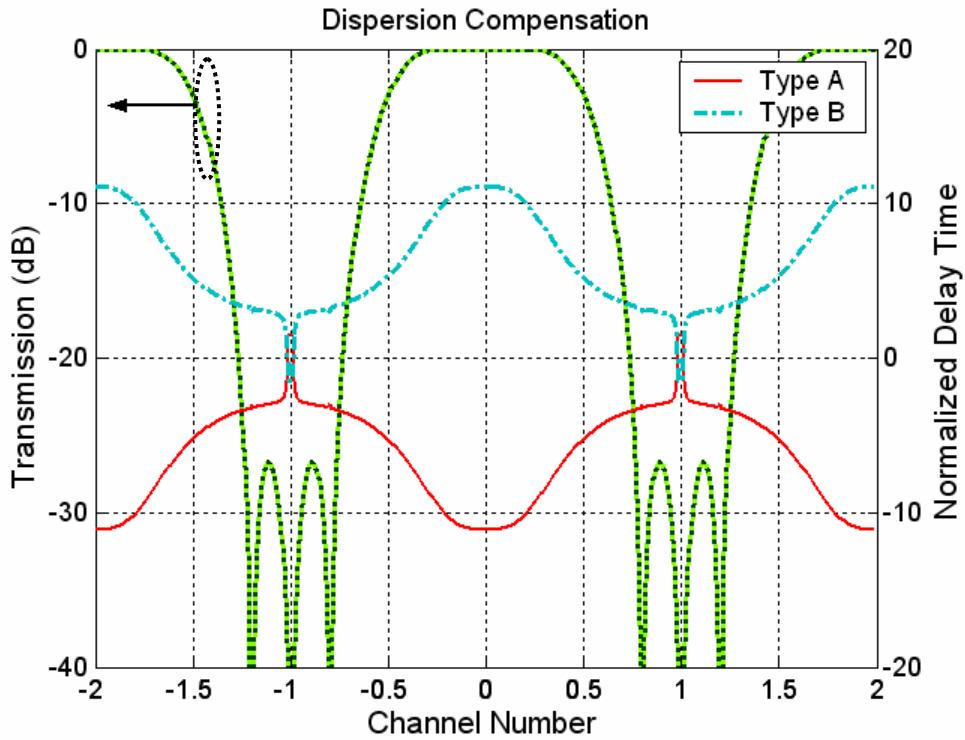


Fig. 2.16 Dispersion compensating interleavers (L-2L-2L) for add/drop node



3. L-2L-4L Interleaver

The found angles for three half-wave plates are 49.8787, -40.3855, and 22.2307 degrees. Figure 2.17 shows the transmission responses of the even and odd channels; the isolation is about 28 dB. The ripple is about 0.0054 dB; the bandwidths of -0.1dB and -0.5dB are $0.6 * df$ (channel spacing) and $0.74 * df$, respectively, as shown in Fig. 2.18. In Fig. 2.19, the type-A and type-B have opposite group delays and company with the same transmission response.

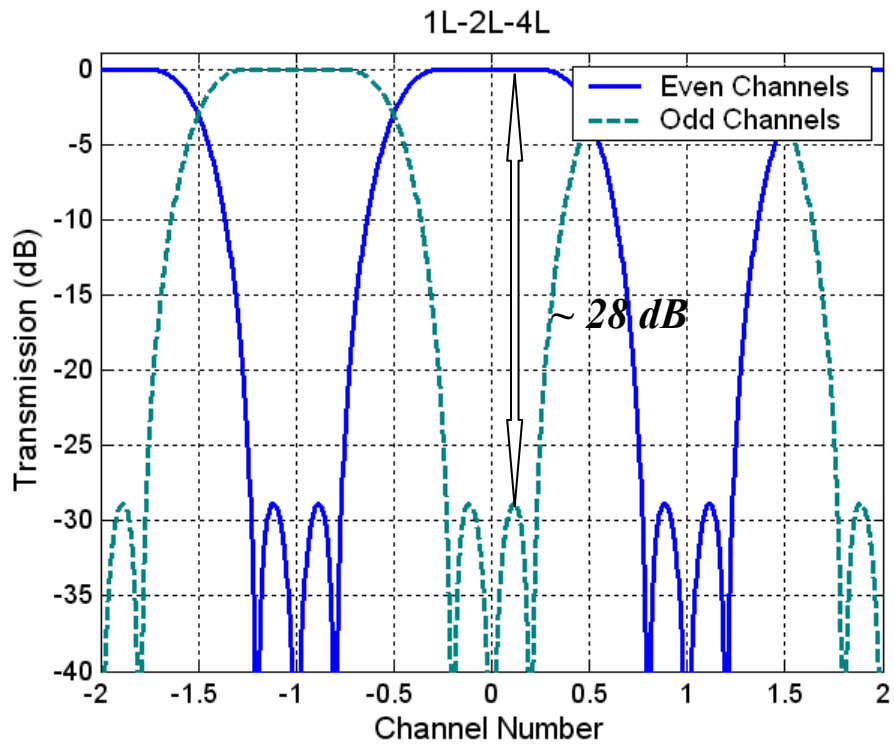


Fig. 2.17 Transmission responses of the even and odd channels

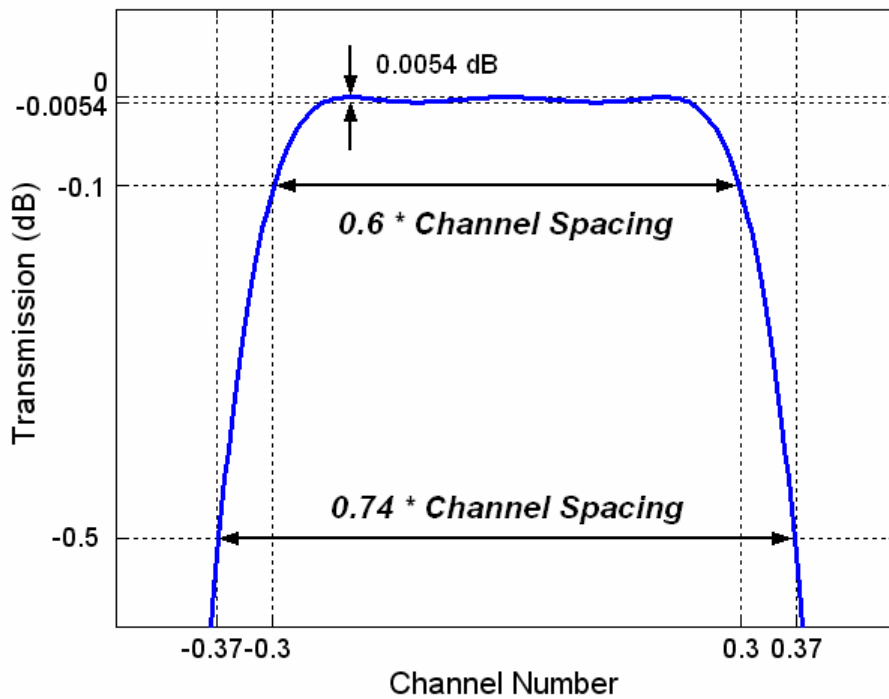


Fig. 2.18 The ripple calculation and the bandwidth estimations of -0.1dB and -0.5dB for L-2L-4L interleaver.

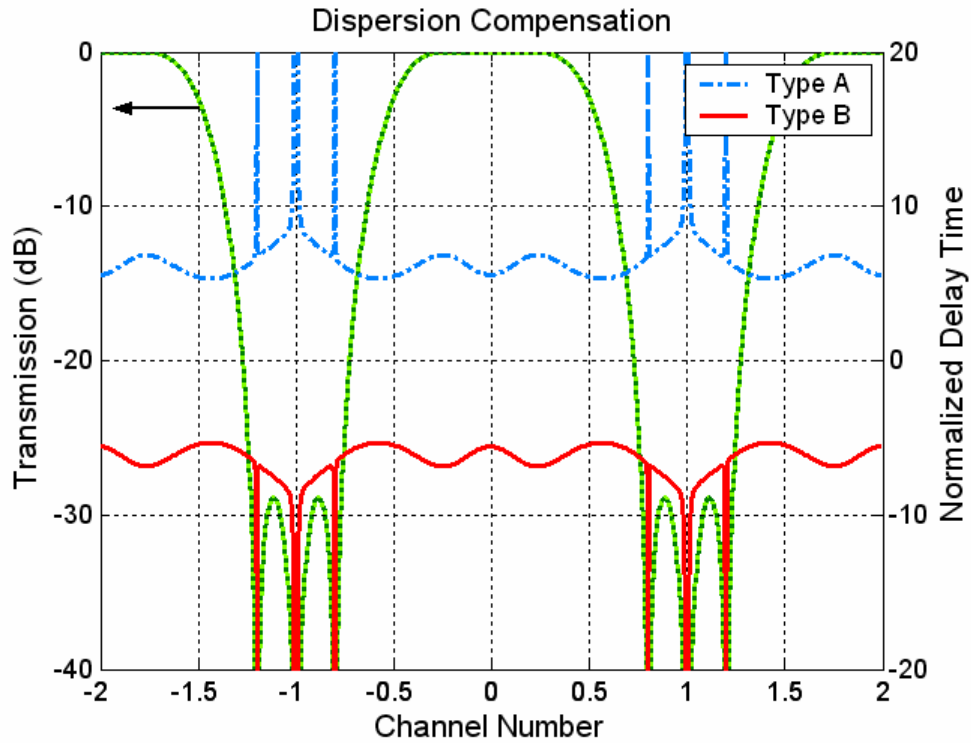


Fig. 2.19 Dispersion compensating interleavers (L-2L-4L) for add/drop node

4. L-2L-2L-2L Interleaver

The found angles for four half-wave plates are 3.9987, 7.9874, 38.4078 and -33.0082 degrees. Figure 2.20 shows the transmission responses of the even and odd channels; the isolation is about 29 dB. The ripple is about 0.0073 dB; the bandwidths of -0.1dB and -0.5dB are $0.6 * df$ (channel spacing) and $0.74 * df$, respectively, as shown in Fig. 2.21. In Fig. 2.22, the type-A and type-B have opposite group delays and company with the same transmission response.

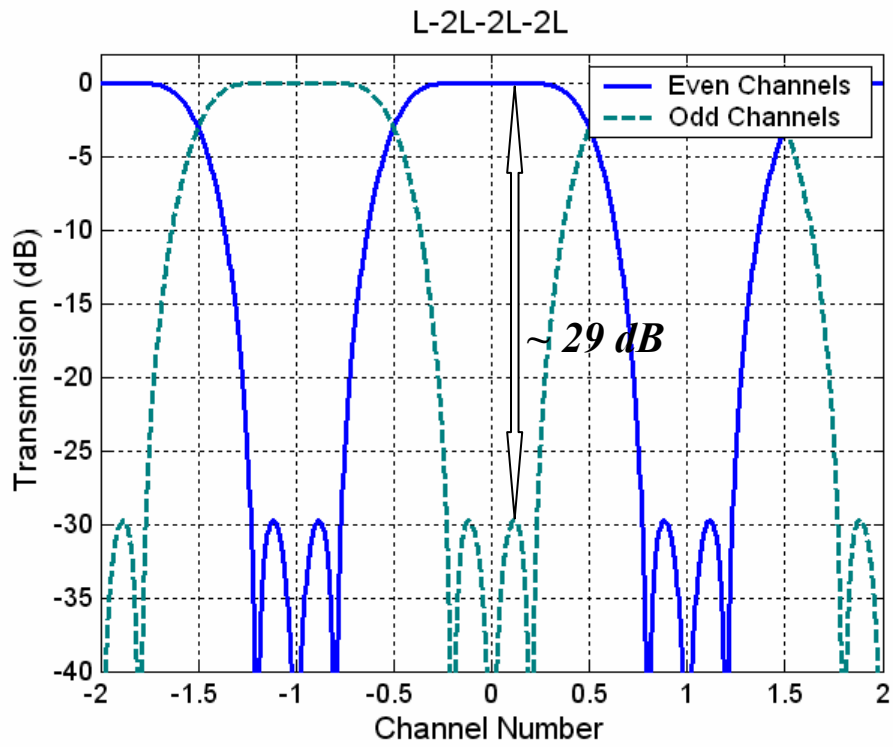


Fig. 2.20 Transmission responses of the even and odd channels

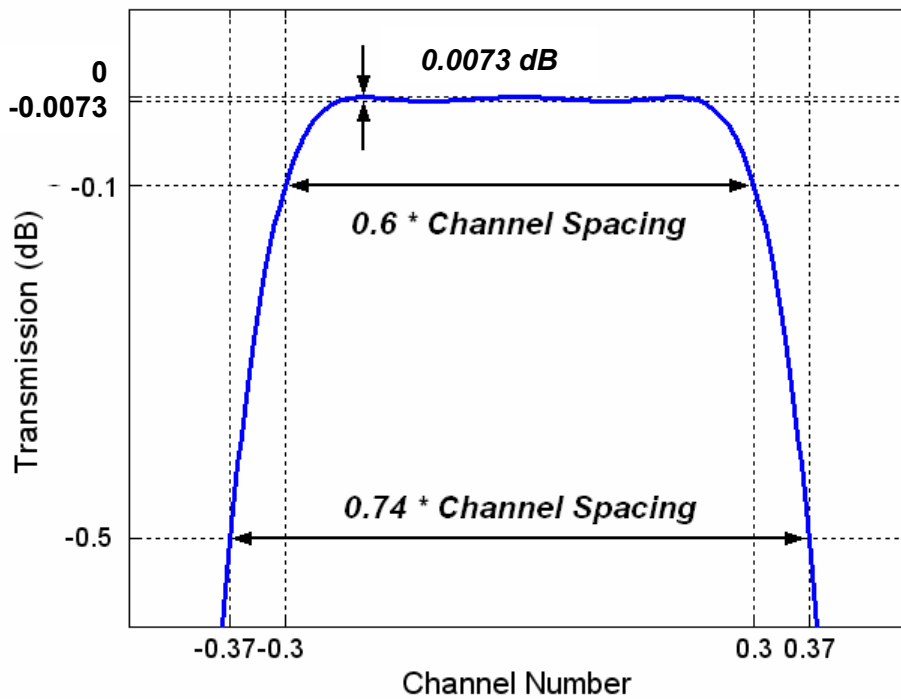


Fig. 2.21 The ripple calculation and the bandwidth estimations of -0.1dB and -0.5dB for L-2L-2L-2L interleaver.

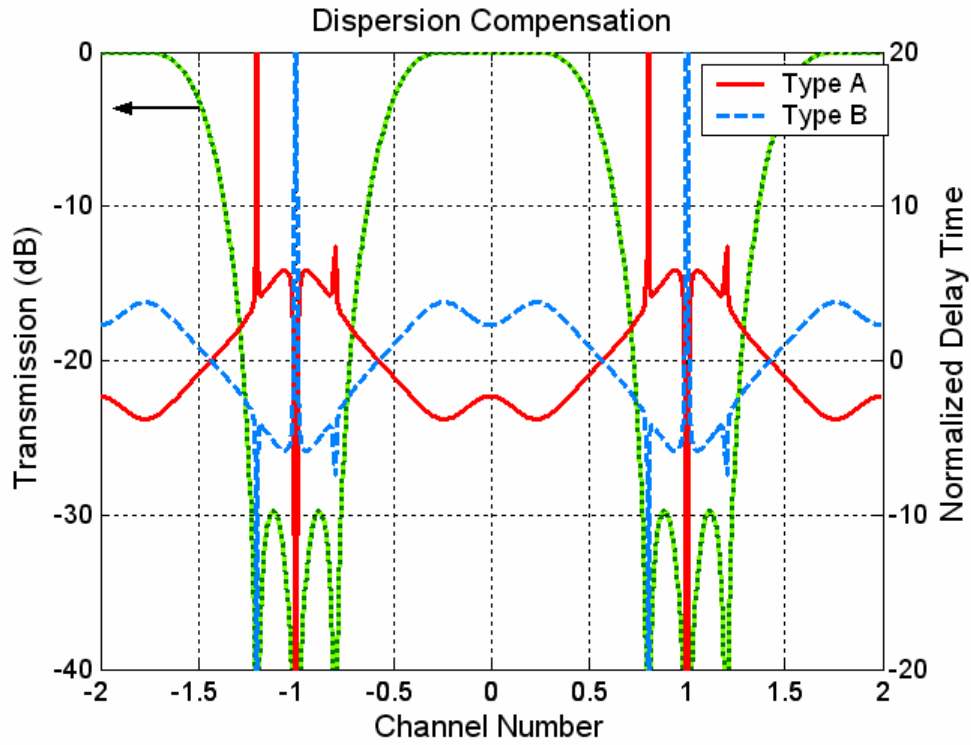


Fig. 2.22 Dispersion compensating interleavers (L-2L-2L-2L) for add/drop node

5. Comparisons

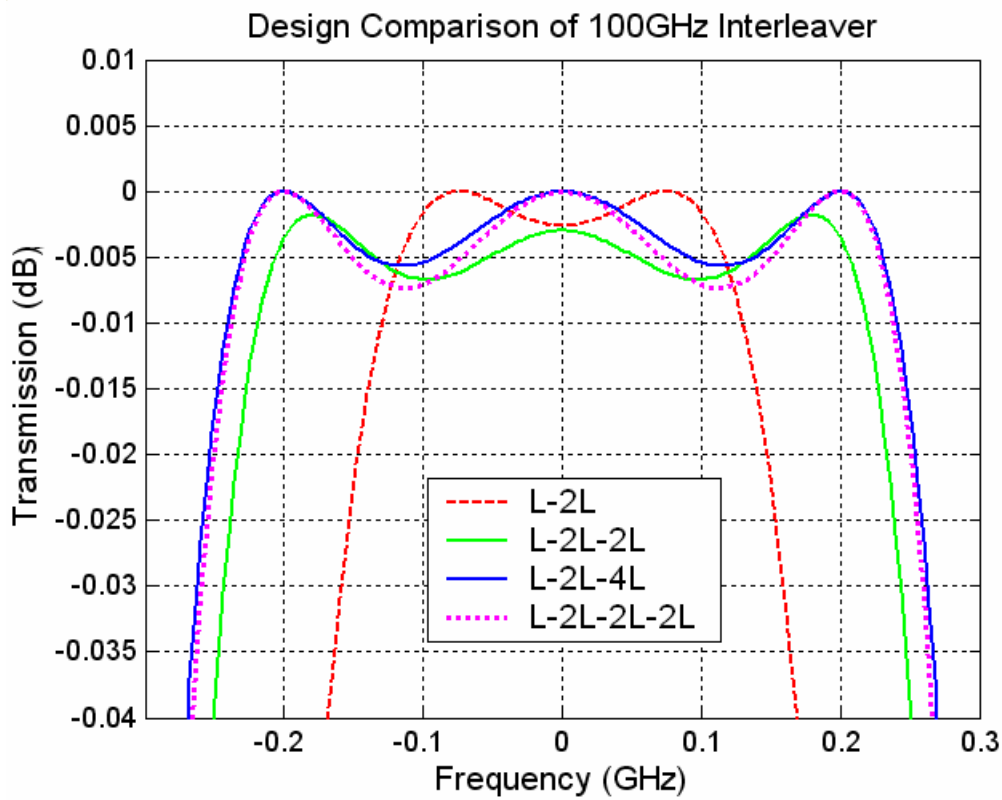


Fig. 2.23 Design comparisons between four types by shape of the top passband.

More delay line stage must be added to increase the highest Fourier frequency edge response; the pass band, the size, and the reliability are all traded off against each other as shown in Fig. 2.23 and Table 2.1. For a 100 GHz interleaver, L-2L-2L can be used to meet the pass band and delay requirements for 40-Gbit/s transmission without difficulty. If only a 10-Gbit/s signal is transmitted, an L-2L design will suffice.

	L-2L	L-2L-2L	L-2L-4L	L-2L-2L-2L
-0.1dB bandwidth	0.41*df	0.58*df	0.6*df	0.6*df
-0.5dB bandwidth	0.61*df	0.72*df	0.74*df	0.74*df
Ripple	0.0026dB	0.0049dB	0.0054dB	0.0073dB
Isolation	-30.5dB	-27dB	-28dB	-29dB

Table 2.1 Comparisons between L-2L, L-2L-2L, L-2L4L, and L-2L-2L-2L interleaves.

2.3.5 Monte-Carlo Simulations

A Monte-Carlo simulation of manufacturing imprecision was conducted to estimate the design tolerance. Two parameters were found to dominate the performance – the lengths of the crystals and the angles of the half-wave plates. The variation of the lengths of crystals and the angles of the half-wave plates were assumed to follow a Gaussian distribution with standard deviations σ of $1 \mu m$ and 1 degree, respectively. Fig. 2.24 and Fig. 2.25 show the simulation results obtained for L-2L-2L-2L interleaver. Figure 2.24 illustrates the weighted amplitude response depends on the Fourier coefficient (Eq. (23)), and the coefficients of the interleaver transfer function depends on the angles of the half-wave plates (Eq. (31)). Figure

2.25 illustrates the channel shift and the variation of channel spacing due to the delay lines depending on the lengths of the crystals.

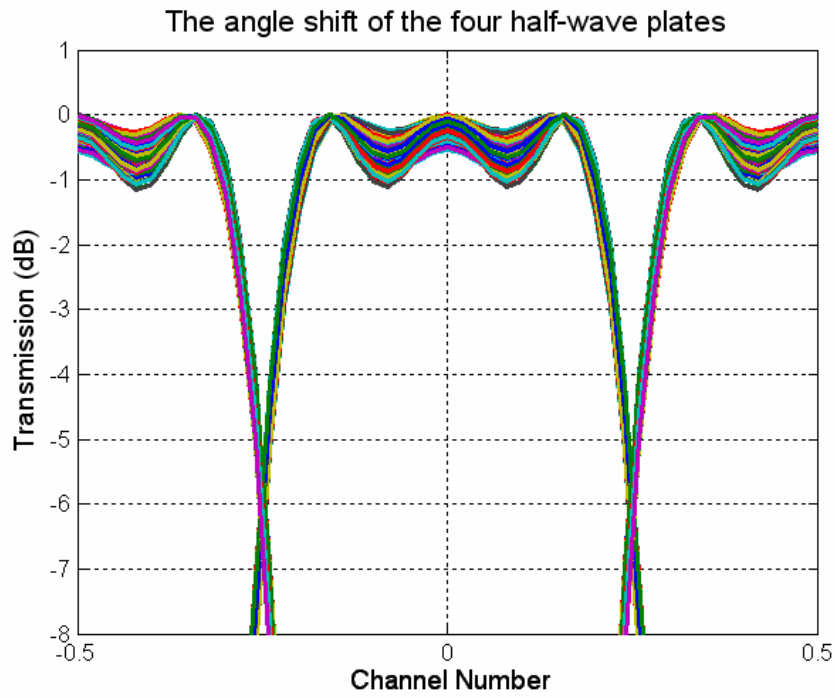


Fig. 2.24 Mote-Carlo simulation for the angle variation

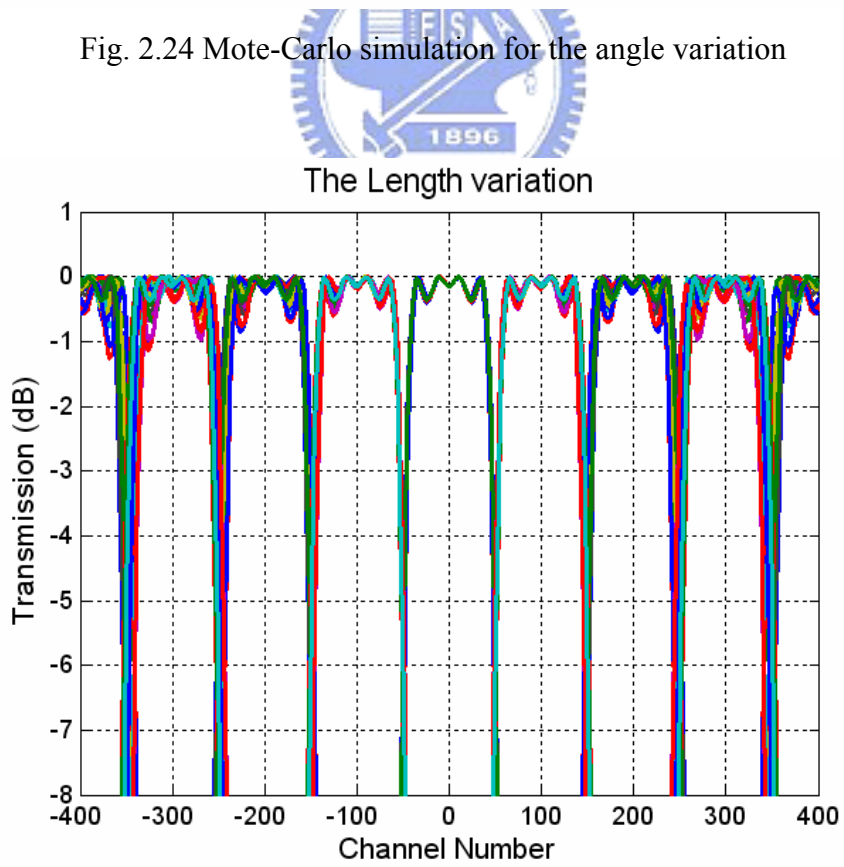


Fig. 2.25 Mote-Carlo simulation for the length variation

2.3.6 Type-AB and Type-AA

In order to simulate and compare the dispersion-free interleaver pairs with non-dispersion-free interleaver pairs in the metro network system, we distinguish them into type-AB and type-AA. Type-AB consists of two interleavers with the opposite group delay, and type-AA consists of two interleavers with the same group delay as shown in Fig. 2.26 and Fig. 2.27. In addition, the transfer function of an interleaver pair will become narrower than that of a single interleaver.

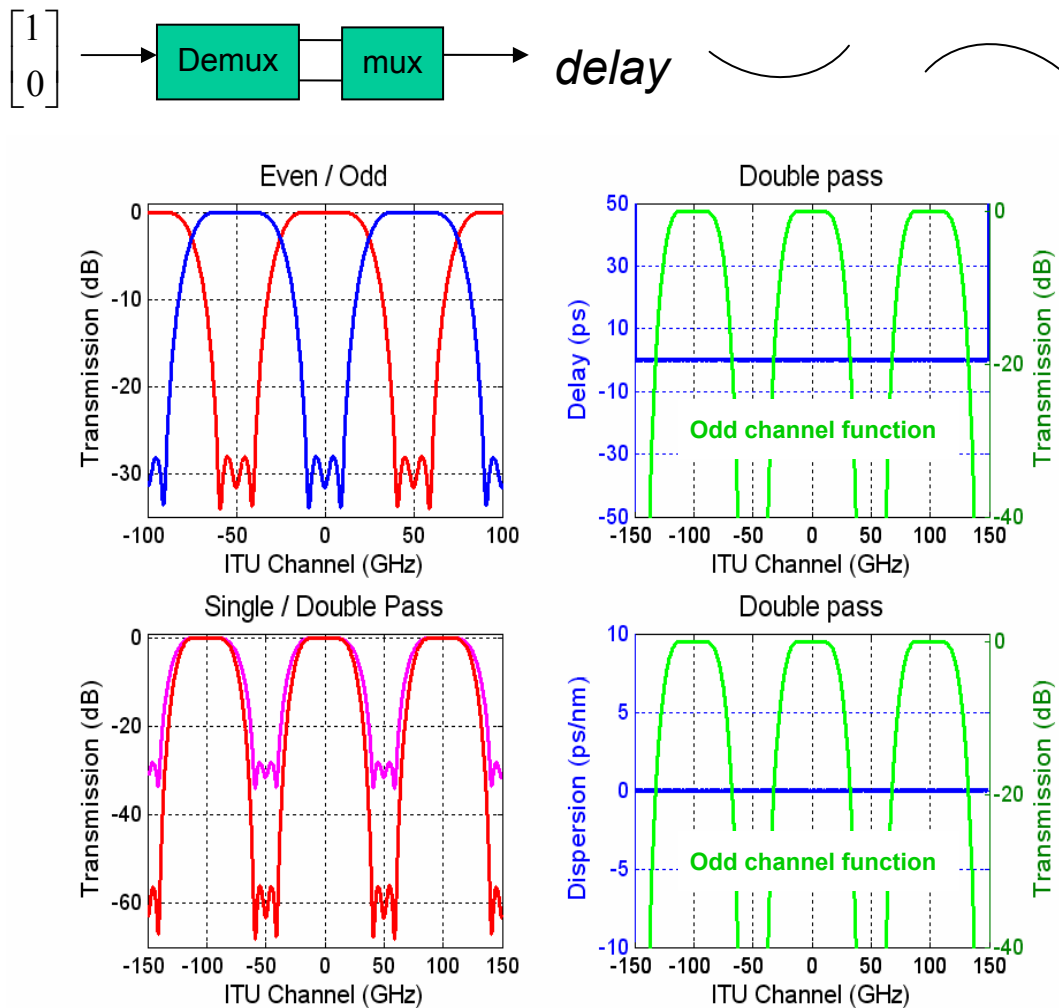


Fig. 2.26 Dispersion Compensated interleaver pair : Type-AB

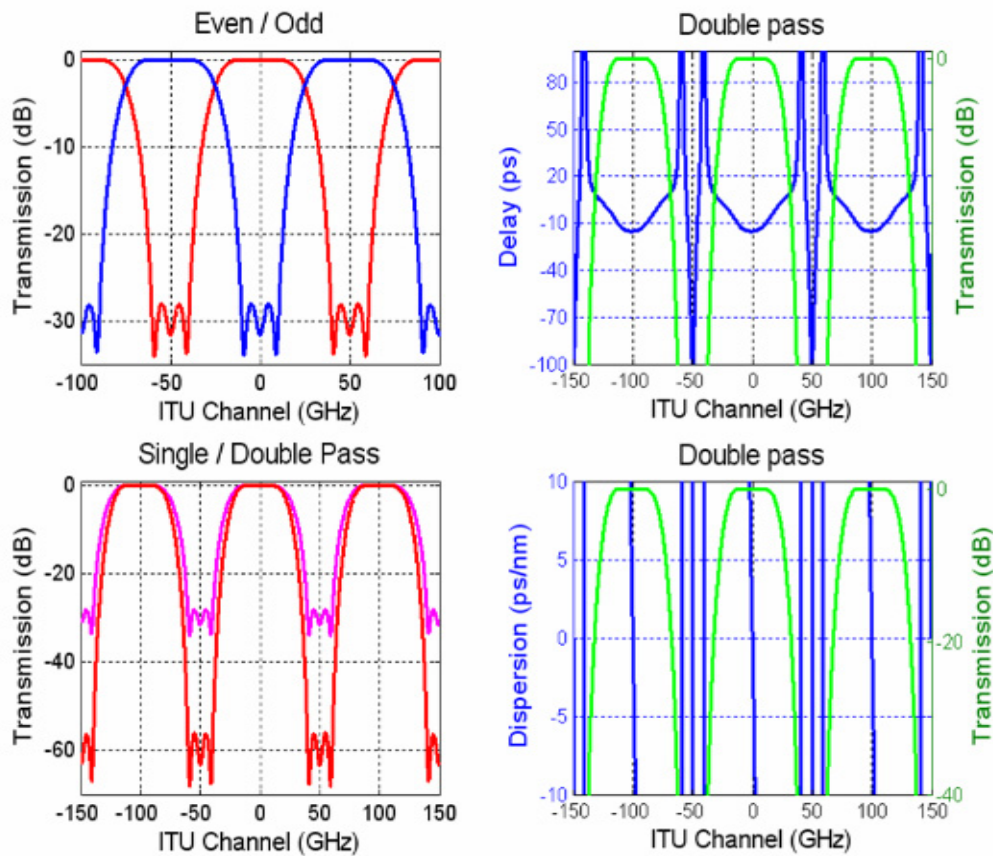
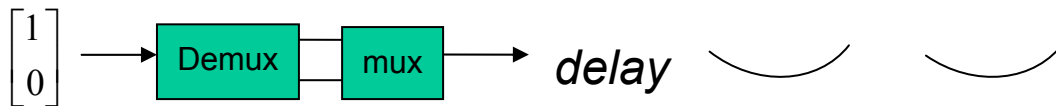


Fig. 2.27 Without Dispersion Compensated interleaver pair : Type-AA

References

[2.1] S. Cao, J. Chen, J. N. Damask, C. R. Doerr, L. Guiziou, G. Harvey, Y. Hibino, S. Suzuki, K.-Y. Wu, P. Xie, “*Interleaver Technology: Comparisons and Applications Requirments,*” *Lightwave Technology, Journal of*, volume: 22 , Issue: 1 , Jan. 2004, pages:281 – 289.

[2.2] Benjamin B. Dingel, “*Properies of a Novel Noncascaded Type, Easy-to-Design,*

Ripple-Free Optical Bandpass Filter,” Journal of Lightwave technology, vol. 19, No. 8. August 1999.

[2.3] A. V. Oppenheim, et al., “*Discrete-Time Signal Processing,*” 2nd ed., Prentice Hall, New Jersey

[2.4] Christi. K. Madsen, Jian H. Zhao, et al., “*Optical Filter Design and Analysis: A Signal Processing Approach,*” Wiley Interscience.

[2.5] A. Oppenheim and R. Schaffer, Digital Signal Processing, 2nd. Ed., Englewood, N.J.: Prentice-Hall, Inc., 1975.

[2.6] Hermann A. Haus, et al., “*Waves and Fields in Optoelectronics,*” Prentice-Hall.

[2.7] A. Yariv, P. Yeh, “*Optical Waves in Crystals,*” Mei Ya.

[2.8] J. Chen, “*Dispersion Compensated Interleaver Pairs for 40 Gb/s Metro Add/Drop Applications,*” Photonics Technology Letters, IEEE, Volume: 16, Issue: 5, May 2004, Pages:1310 – 1312.

[2.9] Gordon E. Carlson, “*Signal and Linear System Analysis,*” wiley.

